Nanoscale

COMMUNICATION

View Article Online
View Journal | View Issue

CrossMark click for updates

Cite this: *Nanoscale*, 2017, **9**, 3375

Received 7th December 2016, Accepted 15th February 2017

DOI: 10.1039/c6nr09459g

rsc.li/nanoscale

Magnetic microkayaks: propulsion of microrods precessing near a surface by kilohertz frequency, rotating magnetic fields†

L. O. Mair,*‡[a] B. A. Evans,‡[b] A. Nacev,[a] P. Y. Stepanov,[a] R. Hilaman,[a] S. Chowdhury,[a] S. Jafari,[a] W. Wang,[c,d] B. Shapiro[e] and I. N. Weinberg[a]

Surface-swimming nano- and micromotors hold significant potential for on-chip mixing, flow generation, sample manipulation, and microrobotics. Here we describe rotating microrods magnetized nearly orthogonally to their long axes. When actuated near a solid surface, these microrods demonstrate precessing motion, with rods describing a double cone similar to the motion of a kayaker's paddle. The precessing motion induces translation. At 1 kHz, these "microkayaks" move at translational velocities of ≈14 μm s^{-1} and generate advective flows up to 10 μm s^{-1}.

Introduction

Magnetic manipulation of micro/nanoscale particles has led to advances in the fields of fluid handling,[1–3] controlled propulsion,[4–6] and cell manipulation.[7–11] Previous work has generated flows above surface walkers,[12] translated non-magnetic particles using rotational flows,[13] trapped particles in local flows,[14] and quantified micromotor rotation by observing local hydrodynamics.[15,16] Rotationally operated microscale rods,[10,14,17] tubes,[18] and helices[19–21] have been implemented for performing various tasks in solution. Template-grown microrods have been propelled *via* catalytic reactions,[22] magnetic gradient pulling,[23] acoustic propulsion,[24–26] dielectrophoretic forces,[27] and end-over-end rotation.[10,14,17]

As these template-grown micromaterials may play a role in nanomedicine/surgery, controlled, high speed manipulation is useful. However, magnetically controlled kilohertz frequency actuation has not been demonstrated. Here we demonstrate controllable, kilohertz frequency motion. We model the resulting translation and demonstrate that precession of the rod around its centerpoint induces translational velocities similar to those we observe experimentally.

Recently, acoustically and optically manipulated microrods have entered the kilohertz operating regime. Acoustically propelled microrods were shown to rotate at ≈2.5 kHz in water, however rotational frequency control was not demonstrated.[15] Optically driven nanorods were actuated at ≈42 kHz in water.[28] Magnetic microrods, on the other hand, have typically remained relegated to frequencies below 100 Hz, and the frequency actuation record for magnetic microrods is currently ≈300 Hz, using magnetic rods attached to pedestals.[29] Here we demonstrate microrods precessing at 1 kHz, which, to the best of our knowledge, is the highest frequency manipulation of magnetic microrods to date. Translation results from symmetry breaking physics due to the rod's proximity to a solid surface.[4,10–12] The precessing motion near the sample floor induces motion akin to a kayaker's paddling, with the rod describing a double cone. Kayaking motion, as opposed to pure rotation around the long axis of the rod, occurs due to the rod's magnetization angles, θ_m, being at a slight angle (≈ 5.4°) with respect to the short axis of the rod.

Near a solid–liquid interface, microrods translate at speeds proportional to rotational drive frequencies, achieving speeds of 14 μm s^{-1} at 1 kHz. Additionally, microrods generate surface flows with observed velocities up to 10 μm s^{-1}. These surface flows arise from local rotational flows induced by microrod rotation, and are visualized by their hydrodynamic impact on polystyrene tracer beads seeded into the sample.

Results

Synthesis and actuation

Microrods are synthesized *via* sequential eletrodeposition of Au–Ni–Au segments (Fig. 1A) into the pores of an anodized aluminium oxide membrane.[26,30,31] Microrods are approxi-

[a]Weinberg Medical Physics, Inc., North Bethesda, Maryland 20817, USA. E-mail: Lamar.Mair@gmail.com
[b]Department of Physics, Elon University, CB# 2625, Elon, North Carolina 27244, USA
[c]School of Material Sciences and Engineering, Harbin Institute of Technology, Shenzhen Graduate School, Shenzhen, China 518055
[d]Center for Soft and Living Matter, Institute of Basic Sciences, Ulsan, Korea
[e]Fischell Department of Bioengineering, University of Maryland, College Park, USA

†Electronic supplementary information (ESI) available: Videos demonstrating rotation, translational motion, microvortices, and advective currents. See DOI: 10.1039/c6nr09459g

‡Equal contribution.

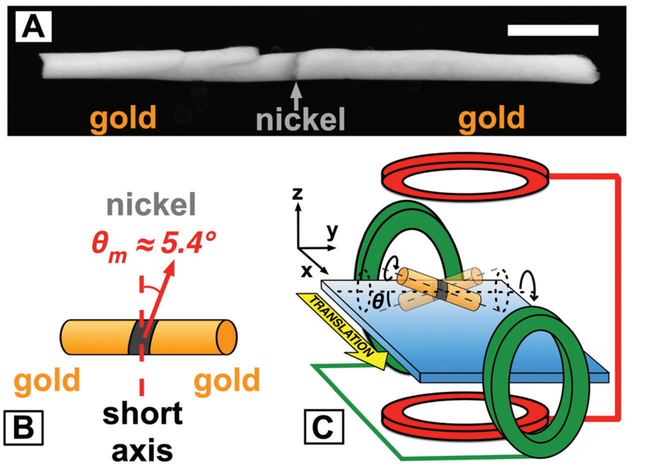

Fig. 1 SEM image of rods and schematic showing rod magnetization and experimental setup. (A) An SEM image of a gold–nickel–gold rod shows the nickel segment tilted slightly with respect to the short axis of the rod. Scale bar is 1 μm. (B) Schematic of rod showing short axis (dashed line) and magnetization angle, θ_m (solid arrow, angle has been exaggerated in drawing). (C) Magnetic coil arrangement shows how rotation (around the rod long axis) and precession (around the *y*-axis) is achieved. The magnetic field orients the long axis of the rod along the *y* direction (at an angle of θ) and rotates the rod in the *xz* plane. Rotation induces rod translation in *x* direction. The rod precesses at $\theta_m \approx 5.4°$.

mately 280 nm in diameter and 5.5 μm long. Microrods contain a thin (≈ 80 nm) nickel segment which is tilted by $\theta_m \approx 5.4° \pm 2.4°$ (mean ± standard deviation for $n = 8$ rods) with respect to the short axis of the rod. The tilted orientation of the nickel segment is due to tilted surfaces in the electroplating setup. Fig. 1B shows the short axis of a rod (dashed vertical line) and the tilted magnetization angle, θ_m (red arrow). Previous reports have demonstrated that electroplated nickel layers shorter than the rod diameter become magnetized along the diameter of the rod.[26,31,32] When dispersed in DI water and deposited in a fluidic chamber having a glass floor and ceiling (0.25 mm height), the rods settle to the floor of the chamber. Experiments are performed in 18 M ohm DI water, and repulsive electrostatic forces between the ionic double layer surrounding the rods and the negatively charged glass floor keeps rods suspended approximately 1 μm above the floor.[11] Two pairs of Helmholtz coils supply a rotating magnetic field in the *x*–*z* plane (Fig. 1C).

Hydrodynamic model of kayaking motion

The applied magnetic field rotates around the *y*-axis. In response to the magnetic field, microrods simultaneously spin (ω_y) around their long axes and precess (kayak) around their centerpoints at an angle of θ with respect to the *y*-axis (Fig. 1C). Here, precessing is caused by the slightly tilted magnetization orientation, θ_m, of the magnetic segment, which is tilted slightly away from the short axis of the rod (Fig. 1B). As a rod precesses, each half of the rod moves alternatingly nearer and farther from the solid–liquid boundary (Fig. 1C). Due to the no-slip boundary condition of the boundary, segments of the rod nearer to the boundary experience more drag than segments of the rod farther from the boundary. The precessing motion induces temporal changes in drag on each segment of the rod. These temporal changes in drag induce translation along the *x*-axis, with translational velocity v_x. Our mathematical model sums the drag on each segment of a rod as it precesses and arrives at a generalized relation for predicting translational velocities (v_x) as a function of rotational velocities (ω_y). The model relies on geometric parameters that impact the relationship between v_x and ω_y. Namely, coupling between rotation (ω_y) and translation (v_x) depends on rod length (L), radius (r), angle of precession with respect to the boundary (θ), and distance from the boundary (d). These geometric parameters are depicted in Fig. 2. In this section we map out our path to the relationship between v_x and ω_y.

Our experiments take place at low Reynolds number (Re ≈ 7×10^{-6}), and forces and torques sum to zero.[33] Meaning, applied magnetic forces and torques are essentially instantaneously balanced by equal and opposite drag forces and torques. The relationship between externally applied forces and torques and resultant translational and rotational velocities may be fully described with a symmetric 6 × 6 resistance matrix, $\boldsymbol{Z}$:

$$\begin{bmatrix} \vec{F} \\ \vec{\tau} \end{bmatrix} = \begin{bmatrix} \boldsymbol{Z_a} & \boldsymbol{Z}_c \\ \boldsymbol{Z}_c^T & \boldsymbol{Z}_b \end{bmatrix} \begin{bmatrix} \vec{v} \\ \vec{\omega} \end{bmatrix}. \quad (1a)$$

In eqn (1a), $\vec{F}$, $\vec{\tau}$, $\vec{v}$, and $\vec{\omega}$ are three-component (x, y, z) vectors representing the net force, net torque, net translational velocity, and net rotational velocity, respectively. In its fully expanded form, eqn (1a) is

$$\begin{bmatrix} F_x \\ F_y \\ F_z \\ \tau_x \\ \tau_y \\ \tau_z \end{bmatrix} = \begin{bmatrix} Z_a^{xx} & Z_a^{xy} & Z_a^{xz} & Z_c^{xx} & Z_c^{xy} & Z_c^{xz} \\ Z_a^{yx} & Z_a^{yy} & Z_a^{yz} & Z_c^{yx} & Z_c^{yy} & Z_c^{yz} \\ Z_a^{zx} & Z_a^{zy} & Z_a^{zz} & Z_c^{zx} & Z_c^{zy} & Z_c^{zz} \\ Z_c^{xx} & Z_c^{yx} & Z_c^{zx} & Z_b^{xx} & Z_b^{xy} & Z_b^{xz} \\ Z_c^{xy} & Z_c^{yy} & Z_c^{zy} & Z_b^{yx} & Z_b^{yy} & Z_b^{yz} \\ Z_c^{xz} & Z_c^{yz} & Z_c^{zz} & Z_b^{zx} & Z_b^{zy} & Z_b^{zz} \end{bmatrix} \begin{bmatrix} v_x \\ v_y \\ v_z \\ \omega_x \\ \omega_y \\ \omega_z \end{bmatrix}. \quad (1b)$$

Here, Z_a terms encompass mass, Z_b terms encompass rotational inertia, and Z_c terms are cross-component terms that describe translation–rotation relationships. Symmetry

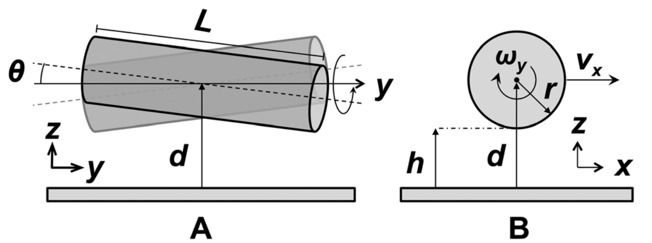

Fig. 2 The geometry of microkayaking. (A) The center point of the rod sits a distance $d \approx 1$ μm above the floor, and the rotating magnetic field induces the rod precessing around the *y*-axis at $\theta \approx 5.4°$. (B) A cross-sectional view of the rod and associated geometric variables: *r* is the radius of the rod, ω_y is the rotational velocity, and v_x is the translational velocity.

must be broken for rotation and translation to be coupled. For spheres,[34–37] ellipsoids,[38,39] and cylinders[40–42] in an unbounded fluid (particles far from a solid–liquid boundary), the cross term $\boldsymbol{Z}_c$ and its transpose $\boldsymbol{Z}_c^T$ are zero and there is no rotational–translational coupling. Thus, in the absence of a boundary, magnetic-field-induced torque would not result in translation. Symmetry breaking can be accomplished by particle shape,[19,33,43,44] or by the presence of a boundary.[4–6,45,46] Introducing a solid or fluid boundary introduces non-zero cross-component $\boldsymbol{Z_c}$ and $\boldsymbol{Z_c^T}$ terms: rotations result in translation, and *vice versa*.

The components of $\boldsymbol{Z}$ incorporate viscosity, drag, and geometry of the rod in motion. Here, viscosity is constant (8.9×10^{-4} cPa s), as the microrod is suspended in water. Drag on each segment of the rod, however, changes as the rod precesses, due to the solid–liquid boundary provided by the floor of the chamber. When rotated around their long axes ($\theta = 0$) at 1 μm above the floor, the upper and lower surfaces of a rod experience slight differences in drag such that rotation around the long axis will generate very slow translational motion (Fig. 3A). However, at $\theta = 0$, the rotation–translation coupling is insufficient to explain the translational velocities we observe.[47] De Corato *et al.* have shown that the rod must be within a few tens of nanometers from the boundary to achieve appreciable translational velocities at 1 kHz.[47] Previous measurements[11] and observations of 1 μm polystyrene beads orbiting rods suggest that the $\theta = 0°$ assumption is a poor choice for assessing the translational velocities we observe. However, precessing motion models predict significant translational velocities at dramatically greater heights above the floor (Fig. 3A) and are more suitable for describing the motion we observe. The magnetization direction of our microrods (Fig. 1A and B) enables precessing in a rotating magnetic field. As a rod precesses, the drag on any segment of the rod oscillates with the segment's proximity to the floor.

For precession about the y direction, only v_x components of velocity are relevant (further details can be found in the ESI†). As applied magnetic forces and torques are balanced by resultant drag forces and torques, we set $\vec{F} = \vec{\tau} = v_y = v_z = \omega_x = \omega_z = 0$. At low Reynolds number, v_x and ω_y sum to zero, taking into account relevant $\boldsymbol{Z}$ terms imposed by proximity to a boundary. We find the relationship between v_x and ω_y by solving the first row of eqn (1b), which yields

$$v_x = -\left(\frac{Z_c^{xy}}{Z_a^{xx}}\right)\omega_y, \quad (2)$$

where v_x has been taken to the other side of eqn (1b).

The relevant coefficients of the resistance matrix, Z_c^{xy} and Z_a^{xx}, are given by Yang and Leal[48] (details are provided in ESI†). These coefficients describe how the strength of coupling between rotation (ω_y) and translation (v_x) depends on rod length (L), radius (r), angle of precession with respect to the boundary (θ), and distance from the boundary (d) (Fig. 2). In general, our model predicts that translation velocity (v_x) increases with increases in precession angle, rod length,

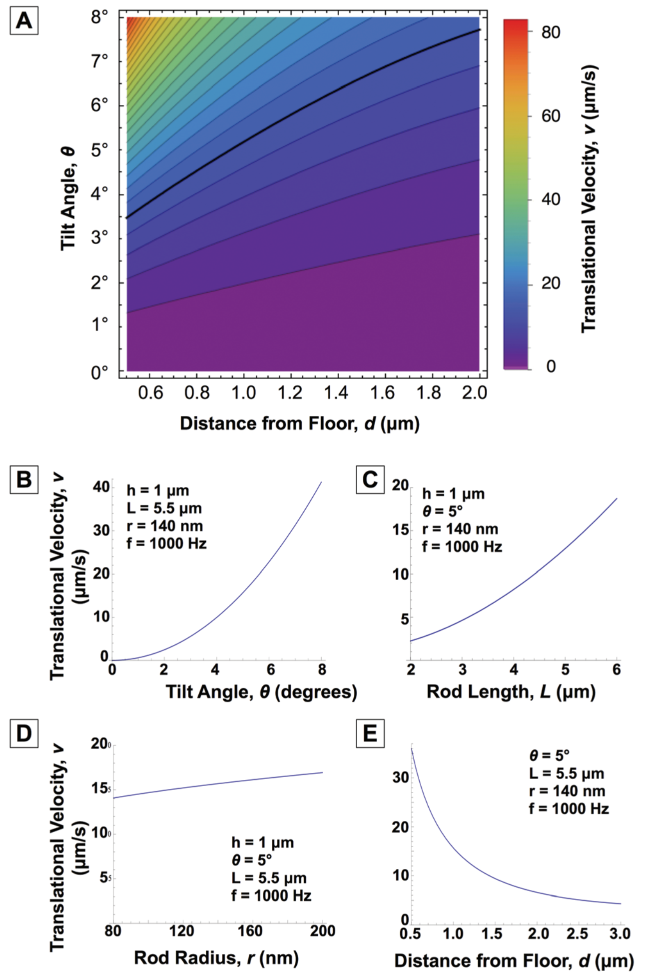

Fig. 3 Predicted translational velocities. Predictions show that for low theta (θ < 1°), translational velocities are small. Additionally, as θ approaches 8° and the rod is moved closer to the surface, translational velocities at 1 kHz approach 80 μm s^{-1}.

radius, or rotation velocity (Fig. 3A–D). Translation velocity decreases as distance from the boundary increases (Fig. 3E).

Expected translational velocities for various values of θ and d are shown in Fig. 3A (for L = 5.5 μm, r = 140 nm), and the kayaking model is in agreement with experimentally observed translational velocities (Fig. 4). The model predicts modest translational velocities (≈ 1 μm s^{-1}) for $\theta = 1°$ and 0.5 μm < d < 2 μm, but predicts translational velocities up to 80 μm s^{-1} for $\theta = 8°$ and d = 0.5 μm (Fig. 3A). Fig. 3B–E predict translational velocities for rods kayaking at 1 kHz with varying values of θ, d, L, and r, respectively.

Experimental validation of the kayaking motion model

Using SEM images we measured $\theta_m = 5.4° \pm 2.4°$, $L \approx 5.5$ μm, and $r \approx 140$ nm. For these parameters at $\theta_m = 5.4°$, the kayaking model predicts velocities of ≈14 μm s^{-1} at 1 kHz (Fig. 3A, bold contour). This model is validated by experimental results demonstrating translational velocities of (13.9 ± 2.7) μm s^{-1} (mean ± standard deviation, measurements based on n = 8) at

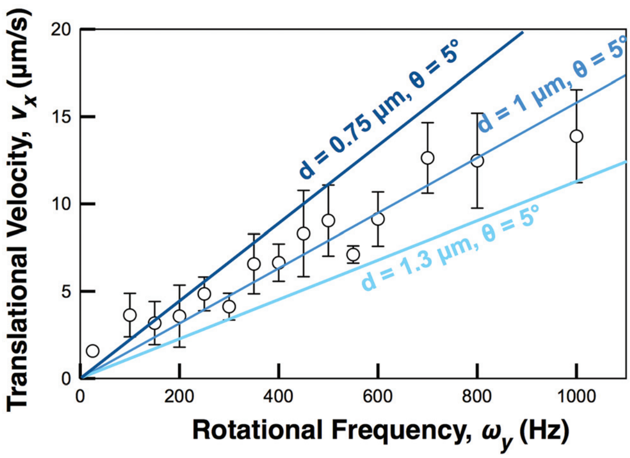

Fig. 4 Experimental translational velocities. A linear frequency–velocity relationship is demonstrated. Error arises from surface asymmetries among various rods, as well as slight rod-to-rod differences in length, radius, tilt angle, and distance above the floor of the sample. Boundaries for the centroid height d are shown.

1 kHz. Expected translational velocities at d = 0.75 μm, 1 μm, and 1.3 μm demonstrate that experimental results are in agreement with predicted values for kayaking rods (Fig. 4). Using the linear frequency–velocity relationship predicted by the kayaking model, we calculate expected velocities for our rods at various tilt angles θ and distances from the floor d (Fig. 3A). We also calculate translation velocities at 1 kHz for various tilt angles θ (Fig. 3B), rod lengths L (Fig. 3C), rod radii r (Fig. 3D), and heights d (Fig. 3E).

Although a precessing slender-body cylinder model confirms our experimental observations, it should be noted that any morphological deviations from a perfect cylinder tend to increase translational velocities. This suggests that our rods may rotate at slightly smaller angles (θ) or at slightly larger distances (d) from the floor and still exhibit velocities consistent with the model (Fig. 4). The relatively large experimental uncertainties associated with translational velocity *versus* rotational frequency data can be attributed to the sensitive nature of the rotation–translation relationship: small deviations in θ, L, or d induce deviations from the expected v_x for a given frequency.

Translational velocities and rotational frequencies

In rotating rods, magnetic fields must perpetually apply torque equivalent to the corresponding rotational drag torque associated with rod rotation. As magnetic field rotation increases, the hydrodynamic drag force on the rod also increases. If the applied magnetic torque is fast but weak, magnetic torque will be insufficient to rotate the rod fast enough to overcome the corresponding viscous drag. When this happens, the rod "steps-out" of phase with the applied magnetic torque. The step-out frequency is the frequency at which the magnetic field strength is insufficient to overcome the hydrodynamic drag on the microrod. Below the step-out frequency, translational motion occurs at a constant velocity. At and above the step-out frequency, the microrod no longer rotates in phase with the applied magnetic field, making translational motion inconsistent.[43,49–52]

Since our image capture frame rate is between one and two orders of magnitude lower than our microrod manipulation frequency, a direct visualization of step-out frequency was not practical. We instead validate step-out frequency by observing microrod behaviour as the driving frequency increased. First, microrods rotated below the step-out frequency appear to glide across the surface at a constant velocity (ESI video†). Below the step-out frequency, the velocity–frequency relationship generally follows $v_x = 1.58 \times 10^{-2}\ \omega_y$, where v_x is in μm s^{-1} and ω_y is in s^{-1} (Fig. 4). Above the step-out frequency, microrods demonstrate highly irregular motion and significantly slowed translation, indicating the translation of the rod is no longer in sync with the rotation of the magnetic field. In our experiment step-out frequency was found to be around 1 kHz.

Rotational flows

As it rotates, each microrod generates its own rotational flow. These rotational flows can entrap and rotate surrounding objects, as evidenced by the advection of a 1 μm diameter polystyrene microsphere momentarily trapped in a rod's rotational flow (Fig. 5 and ESI video†).

Magnetically actuated micro- and nanoscale structures for on-chip flow generation have primarily generated flows using motion in a plane perpendicular to the sample floor.[12,53,54] Detached surface walkers have previously generated flow velocities of 10 μm s^{-1},[12] 12 mm s^{-1},[53] and 1.9 mm s^{-1} (ref. 54) using end-over-end rotation. Here, the kayaking motion generates a rotational flow that is generally shaped like a sheath around the long axis of the microrod. Along the length of the microrod, the flow velocity is nearly uniform (and perpendicular to the rod length) due to θ being small.

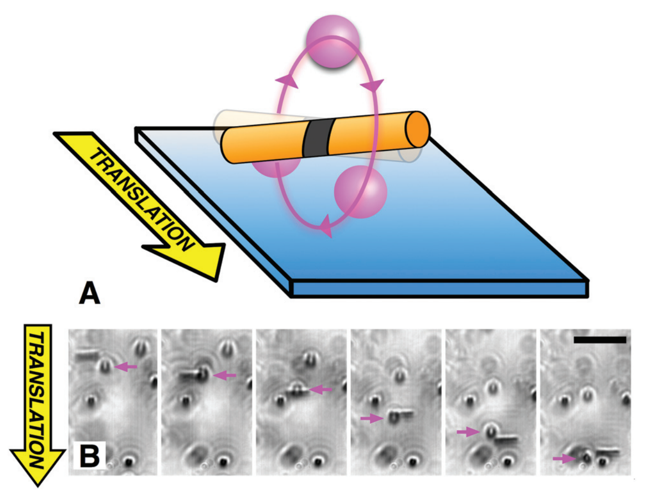

Fig. 5 Demonstration of rotational flows. (A) Cartoon showing a rotating microrod (orange and gray) with an orbiting polystyrene bead (magenta). (B) A microrod's rotation induces a rotational flow around the rod. A polystyrene bead (arrow) is advected in the flow induced by rod rotation, appearing on alternating sides of the rod. Elapsed time between frames is 0.21 s. The scale bar is 10 μm.

Discussion

We achieved rotational frequencies of 1 kHz in a controlled manner, which as far as we know is the fastest magnetically induced rotational motion of motors at this scale. Previous work by Kim *et al.* demonstrated elegant motors attached to posts, capable of rotational frequencies up to 300 Hz in a controlled manner. Acoustically propelled microrods were previously recorded spinning at 2.5 kHz, however, the rate of rotation was uncontrolled, with measurements suggesting that rotational frequencies varied from 0.5 kHz to 2.5 kHz.[15] Future applications to the fields of microfluidics, micromanipulation, and mixing may make use of ultrafast magnetic microrods spinning with fully controlled frequencies.

Previous magnetic particle based flow generators have been rotated end-over-end, generating flow fields with dimensions proportional to the diameter of the rod or bead assembly. Here, the geometry of rotating microrods means each microrod generates a flow sheet spanning the length of the rod. Previous work by Tung *et al.* generated flow sheets using lithographically fabricated rectangular prisms (300 μm × 60 μm × 50 μm), which were rotated at 10–20 Hz.[55,56]

Previous work ablating thrombi using rotationally manipulated magnetic swarms[57] and disrupting biofilms using rotating microrods[58] suggests that rotating particles at high speed can perform significant mechanical work in biological settings. The high frequencies obtained by our microrods indicate it may be possible to accelerate ablation processes using kilohertz frequency motion. Additionally, axial rotational manipulation of ellipsoidal particles may hold promise for moving through viscoelastic biopolymers such as mucus.[59,60] The bacteria *Caulobacter crescentus* makes use of a similar precessing motion, and Liu *et al.* recently concluded that precession of these bacteria enhances motility.[61]

Conclusions

We demonstrate kilohertz frequency rotation using magnetic fields, achieving the fastest magnetically induced, controlled frequency spinning of microrods to date. Detailed inspection of hydrodynamic geometric parameters elucidates a novel, near-surface kayaking motion which generates translational motion, flow sheets above the motors, and microvortices around the motors through symmetry breaking by substrate. Additionally, these microrods are the first sub-10 μm rods demonstrating translational motion orthogonal to their long axes. Potential applications for these devices include lab on chip mixing, flow generation, and particle manipulation.

Acknowledgements

We acknowledge the support of the Maryland NanoCenter, its Fablab, and its NispLab. Additionally, we acknowledge the support of the Georgetown University Nanoscience and Microtechnology Laboratory (GNuLab).

Notes and references

1 S. L. Biswal and A. P. Gast, Micromixing with linked chains of paramagnetic particles, *Anal. Chem.*, 2004, **76**, 6448–6455.
2 A. R. Shields, *et al.*, Biomimetic cilia arrays generate simultaneous pumping and mixing regimes, *Proc. Natl. Acad. Sci. U. S. A.*, 2010, **107**, 15670–15675.
3 B. L. Fiser, A. R. Shields, M. R. Falvo and R. Superfine, Highly responsive core-shell microactuator arrays for use in viscous and viscoelastic fluids, *J. Micromech. Microeng.*, 2015, **25**, 025004.
4 P. Tierno, T. H. Johansen and T. M. Fischer, Magnetically driven colloidal microstirrer, *J. Phys. Chem. B*, 2007, **111**, 3077–3080.
5 O. Güell, F. Sagués and P. Tierno, Magnetically driven Janus micro-ellipsoids realized via asymmetric gathering of the magnetic charge, *Adv. Mater.*, 2011, **23**, 3674–3679.
6 P. Tierno and F. Sagués, Steering trajectories in magnetically actuated colloidal propellers, *Eur. Phys. J. E: Soft Matter Biol. Phys.*, 2012, **35**, 9748.
7 A. Hultgren, M. Tanase, C. S. S. Chen, G. J. J. Meyer and D. H. H. Reich, Cell manipulation using magnetic nanowires, *J. Appl. Phys.*, 2003, **93**, 7554–7556.
8 M. Tanase, *et al.*, Assembly of multicellular constructs and microarrays of cells using magnetic nanowires, *Lab Chip*, 2005, **5**, 598–605.
9 Y. Zhao and H. Zeng, Rotational maneuver of ferromagnetic nanowires for cell manipulation, *IEEE Trans. Nanobioscience*, 2009, **8**, 226–236.
10 L. Zhang, *et al.*, Controlled propulsion and cargo transport of rotating nickel nanowires near a patterned solid surface, *ACS Nano*, 2010, **4**, 6228–6234.
11 L. O. Mair, *et al.*, Highly controllable near-surface swimming of magnetic Janus nanorods: application to payload capture and manipulation, *J. Phys. D: Appl. Phys.*, 2011, **44**, 125001.
12 C. E. Sing, L. Schmid, M. F. Schneider, T. Franke and A. Alexander-Katz, Controlled surface-induced flows from the motion of self-assembled colloidal walkers, *Proc. Natl. Acad. Sci. U. S. A.*, 2010, **107**, 535–540.
13 Z. Ye, E. Diller and M. Sitti, Micro-manipulation using rotational fluid flows induced by remote magnetic micromanipulators, *J. Appl. Phys.*, 2012, **112**, 064912.
14 T. Petit, L. Zhang, K. E. Peyer, B. E. Kratochvil and B. J. Nelson, Selective trapping and manipulation of microscale objects using mobile microvortices, *Nano Lett.*, 2012, **12**, 156–160.
15 A. L. Balk, *et al.*, Kilohertz Rotation of Nanorods Propelled by Ultrasound, Traced by Microvortex Advection of Nanoparticles, *ACS Nano*, 2014, **8**, 8300–8309.
16 W. Wang, W. Duan, A. Sen and T. E. Mallouk, Catalytically powered dynamic assembly of rod-shaped nanomotors and passive tracer particles, *Proc. Natl. Acad. Sci. U. S. A.*, 2013, **110**, 17744–17749.

17 L. Zhang, T. Petit, K. E. Peyer and B. J. Nelson, Targeted cargo delivery using a rotating nickel nanowire, *Nanomedicine*, 2012, 1–7, DOI: 10.1016/j.nano.2012.03.002.
18 W. Xi, *et al.*, Rolled-up magnetic microdrillers: towards remotely controlled minimally invasive surgery, *Nanoscale*, 2013, **5**, 1–4.
19 A. Ghosh and P. Fischer, Controlled propulsion of artificial magnetic nanostructured propellers, *Nano Lett.*, 2009, **9**, 2243–2245.
20 L. Zhang, K. E. Peyer and B. J. Nelson, Artificial bacterial flagella for micromanipulation, *Lab Chip*, 2010, **10**, 2203–2215.
21 J. Li, *et al.*, Template electrosynthesis of tailored-made helical nanoswimmers, *Nanoscale*, 2013, **6**, 9415–9420.
22 W. F. Paxton, *et al.*, Catalytic Nanomotors : Autonomous Movement of Striped Nanorods, *J. Am. Chem. Soc.*, 2004, **126**, 13424–13431.
23 J. A. Cribb, T. D. Meehan, S. M. Shah, K. Skinner and R. Superfine, Cylinders vs. Spheres : Biofluid Shear Thinning in Driven Nanoparticle Transport, *Ann. Biomed. Eng.*, 2010, **38**, 3311–3322.
24 W. Wang, L. A. Castro, M. Hoyos and T. E. Mallouk, Autonomous Motion of Metallic Micro-rods Propelled by Ultrasound, *ACS Nano*, 2012, **6**, 6122–6132.
25 V. Garcia-Gradilla, *et al.*, Functionalized Ultrasound-Propelled Magnetically Guided Nanomotors: Toward Practical Biomedical Applications, *ACS Nano*, 2013, **7**, 9232–9240.
26 S. Ahmed, *et al.*, Steering Acoustically Propelled Nanowire Motors toward Cells in a Biologically Compatible Environment Using Magnetic Fields, *Langmuir*, 2013, **29**, 16113–16118.
27 P. Calvo-marzal, *et al.*, Propulsion of nanowire diodes, *Chem. Commun.*, 2010, **46**, 1623–1624.
28 L. Shao, Z.-J. Yang, D. Andren, P. Johansson and M. Kall, Gold Nanorod Rotary Motors Driven by Resonant Light Scattering, *ACS Nano*, 2015, **9**, 12542–12551.
29 K. Kim, X. Xu, J. Guo and D. L. Fan, Ultrahigh-speed rotating nanoelectromechanical system devices assembled from nanoscale building blocks, *Nat. Commun.*, 2014, **5**, 3632.
30 C. R. Martin, Nanomaterials: A Membrane-Based Approach Synthetic Approach, *Science*, 1994, **266**, 1961–1966.
31 J. C. Love, A. R. Urbach, M. G. Prentiss and G. M. Whitesides, Three-Dimensional Self-Assembly of Metallic Rods with Submicron Diameters Using Magnetic Interactions, *J. Am. Chem. Soc.*, 2003, **125**, 12696–12697.
32 L. T. Schelhas, M. J. Banholzer, C. A. Mirkin and S. H. Tolbert, Magnetic confinement and coupling in narrow-diameter Au–Ni nanowires, *J. Magn. Magn. Mater.*, 2015, **379**, 239–243.
33 E. M. M. Purcell, Life at low Reynolds number, *Am. J. Phys.*, 1977, **45**, 3–11.
34 W. R. Dean and M. E. O'Neill, A slow motion of viscous liquid caused by the rotation of a solid sphere, *Mathematika*, 1963, **10**, 13–24.
35 A. J. Goldman, R. G. Cox and H. Brenner, Slow Viscous Motion of a Sphere Parallel to a Plane Wall I: Motion through a Quiscent Fluid, *Chem. Eng. Sci.*, 1967, **22**, 637–651.
36 S. H. Lee and L. G. Leal, Motion in the Presence of a plane interface 2: An exact solution in bipolar coordinates, *J. Fluid Mech.*, 1980, **98**, 193–224.
37 M. Chaoui and F. Feuillebois, Creeping flow around a sphere in a shear flow close to a wall, *Q. J. Mech. Appl. Math.*, 2003, **56**, 381–410.
38 D. J. Jeffrey and Y. Onishi, The slow motion of a cylinder next to a plane wall, *Q. J. Mech. Appl. Math.*, 1981, **34**, 129–137.
39 J. Yang, G. Huber and C. W. Wolgemuth, Forces and Torques on Rotating Spirochete Flagella, *Phys. Rev. Lett.*, 2011, **107**, 268101.
40 E. Gavze and M. Shapiro, Particles in a shear flow near a solid wall: Effect of nonsphericity on forces and velocities, *Int. J. Multiphase Flow*, 1997, **23**, 155–182.
41 R. Hsu and P. Ganatos, The motion of a rigid body in viscous-fluid bounded by a plane wall, *J. Fluid Mech.*, 1989, **207**, 29–72.
42 R. Hsu and P. Ganatos, Gravitational and zero-drag motion of a spheroid adjacent to an inclined plane at low-Reynolds Number, *J. Fluid Mech.*, 1994, **268**, 267–292.
43 J. J. Abbott, *et al.*, How Should Microrobots Swim?, *Int. J. Rob. Res.*, 2009, **28**, 1434–1447.
44 L. Zhang, *et al.*, Characterizing the swimming properties of artificial bacterial flagella, *Nano Lett.*, 2009, **9**, 3663–3667.
45 P. Tierno, R. Golestanian, I. Pagonabarraga and F. Sagués, Controlled swimming in confined fluids of magnetically actuated colloidal rotors, *Phys. Rev. Lett.*, 2008, **101**, 218304.
46 P. Tierno, J. Claret, F. Sagués and A. Cēbers, Overdamped dynamics of paramagnetic ellipsoids in a precessing magnetic field, *Phys. Rev. E: Stat. Phys., Plasmas, Fluids, Relat. Interdiscip. Top.*, 2009, **79**, 1–6.
47 M. De Corato, F. Greco, G. D'Avino and P. L. Maffettone, Hydrodynamics and Brownian motions of a spheroid near a rigid wall, *J. Chem. Phys.*, 2015, **142**, 194901.
48 Y. G. Yang and L. G. Leal, Particle Motion in Stokes-Flow Near a Plane Fluid Fluid Interface. 1. Slender Body in a Quiescent Fluid, *J. Fluid Mech.*, 1983, **136**, 393/421.
49 A. Ghosh, P. Mandal, S. Karmakar and A. Ghosh, Analytical theory and stability analysis of an elongated nanoscale object under external torque, *Phys. Chem. Chem. Phys.*, 2013, **15**, 10817–10823.
50 K. E. Peyer, L. Zhang and B. J. Nelson, Bio-inspired magnetic swimming microrobots for biomedical applications, *Nanoscale*, 2013, **5**, 1259–1272.
51 F. Meshkati and H. C. Fu, Modeling rigid magnetically rotated microswimmers: Rotation axes, bistability, and controllability, *Phys. Rev. E: Stat. Phys., Plasmas, Fluids, Relat. Interdiscip. Top.*, 2014, **90**, 1–11.
52 P. L. Venugopalan, *et al.*, Conformal cytocompatible ferrite coatings facilitate the realization of a nanovoyager in human blood, *Nano Lett.*, 2014, **14**, 1968–1975.

53 M. Karle, *et al.*, Controlled counter-flow motion of magnetic bead chains rolling along microchannels, *Microfluid, Nanofluidics*, 2010, **10**, 935–939.
54 Y. Gao, *et al.*, Strong vortical flows generated by the collective motion of magnetic particle chains rotating in a fluid cell, *Lab Chip*, 2015, **15**, 351–360.
55 H.-W. Tung, K. E. Peyer, D. F. Sargent and B. J. Nelson, Noncontact manipulation using a transversely magnetized rolling robot, *Appl. Phys. Lett.*, 2013, **103**, 114101.
56 H. W. Tung, D. F. Sargent and B. J. Nelson, Protein crystal harvesting using the RodBot: A wireless mobile microrobot, *J. Appl. Crystallogr.*, 2014, **47**, 692–700.
57 J. L. F. Gabayno, D. Liu, M. Chang and Y. Lin, Controlled manipulation of Fe3O4 nanoparticles in an oscillating magnetic field for fast ablation of microchannel occlusion, *Nanoscale*, 2015, **7**, 3947–3953.
58 L. O. Mair, *et al.*, Biofilm disruption with rotating microrods enhances antimicrobial efficacy, *J. Magn. Magn. Mater.*, 2017, **427**, 81–84.
59 D. Schamel, *et al.*, Nanopropellers and Their Actuation in Complex Viscoelastic Media, *ACS Nano*, 2014, **8**, 8794–8801.
60 D. Walker, B. T. Käsdorf, H. Jeong, O. Lieleg and P. Fischer, Enzymatically active biomimetic micropropellers for the penetration of mucin gels, *Sci. Adv.*, 2015, **1**, e1500501.
61 B. Liu, *et al.*, Helical motion of the cell body enhances Caulobacter crescentus motility, *Proc. Natl. Acad. Sci. U. S. A.*, 2014, **111**, 11252–11256.